International Journal of Hydrogen Energy 210 (2026) 153578

Contents lists available at ScienceDirect

International Journal of Hydrogen Energy

journal homepage: www.elsevier.com/locate/he

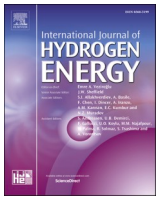

Hydrogen reactivity with wellbore and polymer-modified cements: experimental insights for safe underground hydrogen storage

Sebastian Bruckschlögl [a,*], Chaojie Cheng [b], Peter Thissen [a], Benjamin Busch [b], Christoph Hilgers [b], Frank Dehn [a]

[a] Institute of Concrete Structures and Building Materials (IMB), KIT – Karlsruhe Institute of Technology, Gotthard-Franz-Str. 3, Bldg. 50.31, 76131, Karlsruhe, Germany
[b] Structural Geology and Tectonics, Institute of Applied Geosciences (AGW), KIT – Karlsruhe Institute of Technology, Adenauerring 20a, Bldg. 50.40, 76131, Karlsruhe, Germany

ARTICLE INFO

Keywords:
Wellbore cement
Polymer-modified cement
Underground hydrogen storage
Batch experiments
Well integrity
Microstructure

ABSTRACT

Underground Hydrogen Storage (UHS) is a promising approach to store energy in large quantities to balance the fluctuation between renewable energy supply and overall energy demand. Compared to established underground natural gas storage, UHS imposes stricter requirements on gas tightness and long-term well integrity, which must be thoroughly investigated before implementation. While thermodynamic modelling suggests potential chemical reactions relevant to long-term stability, experimental data remain limited. Additionally, no studies have investigated polymer-modified cements, which exhibit promising material properties to meet the increased requirements. This study investigates the reactivity of hardened wellbore cement paste and polymer-modified cement paste with hydrogen under conditions of 50 °C and 100 bar over 4 weeks. To examine the individual effects of gas, temperature, and pressure on the reactivity, a combination of microstructural and mineralogical analyses, along with mechanical and physical properties evaluations, was conducted under various exposure conditions. The results indicate no detectable reactivity between hydrogen and the tested cement materials, supporting the feasibility of long-term and safe UHS using wellbore cements.

1. Introduction

To support a climate-friendly energy transition and conserve natural resources, the shift towards renewable energy is accelerating. However, the intermittent nature of wind and solar power requires efficient energy storage to ensure grid stability. Hydrogen produced via electrolysis is a promising universal energy carrier for future storage systems. Among various storage options, Underground Hydrogen Storage (UHS) stands out due to its large-scale capacity (GWh to TWh) [1,2]. Although UHS can leverage insights from the well-established natural gas storage and oil and gas operations, it brings unique challenges, particularly regarding gas-tightness and long-term material stability when in contact with hydrogen [3]. Wellbore sealing is typically achieved using cement slurries, whose chemical stability depends on temperature, pressure, humidity, brine/gas composition, and mineral presence.

Class G cement, a Portland cement defined by API SPEC 10 A [4], is widely used due to its adaptability across subsurface conditions [5]. The slurry composition is adjusted with small quantities of additives to meet the required density, viscosity and strength development. Ordinary Portland Cement (OPC) mainly consists of the oxide phases: alite (C_3S), belite (C_2S), tricalcium aluminate (C_3A), calcium aluminoferrite/-brownmillerite (C_4AF), and small quantities of gypsum. Mixed with water those phases hydrate to form calcium hydroxide - also known as portlandite (CH), calcium-silicate-hydrates (C–S–H) and some ettringite (most dominant representative of AFt and stable below 60 °C [6]). These hydration products can transform into monosulfoaluminate (dominant sulfate form of AFm phases), depending on pH value and temperature.

Rock-fluid and cement-fluid geochemical interactions in different underground environments are investigated intensively [3,6]. Among known degradation mechanisms for cement, carbonation—driven by dissolved CO_2—plays a key role, dissolving CH and C–S–H and precipitating calcite and amorphous silica gel [7]. Despite this, the degradation process is typically slow and field studies (e.g., Carey et al. [8]) show well integrity can be maintained for decades under high CO_2 exposure.

However, UHS is a relatively new application and knowledge to potential chemical interactions between hydrogen and hardened cement

* Corresponding author.
E-mail address: sebastian.bruckschloegl@kit.edu (S. Bruckschlögl).

https://doi.org/10.1016/j.ijhydene.2026.153578
Received 26 October 2025; Received in revised form 12 January 2026; Accepted 14 January 2026
Available online 24 January 2026

paste are limited. A summary of existing studies is provided in Supplementary Materials (SM-Table S1). Thermodynamic modelling can serve as the basis for in-depth investigations, describing the following potential reactions:

- **Stability of main phases:** CH and C–S–H remain stable in the absence of CO_2 [9,10]. In the presence of CO_2, they gradually convert to calcite, which can further be dissolved under excess CO_2 [7] or hydrogen [10].
- **Minor phase transformations:** Remaining C_3A and C_4AF could transform to hydrogarnet (C_3AH_6) [10], while C_4AF may also convert to mackinawite with sulfides (FeS) and magnetite (Fe_3O_4) instead of maghemite [10]. Hematite (Fe_2O_3) can be dissolved [9] and transform to magnetite (Fe_3O_4) [11], though this is unlikely below 300 °C [12].
- **Sulfate reduction:** Sulfates (SO_4^{2-}) in (remaining) gypsum, monosulfoaluminate [10] and ettringite [9] may be reduced to sulfides (S^{2-}) and dissolved, which can precipitate with ferrous iron as mackinawite (FeS) [9].
- **Microbial influence:** Microorganisms could enhance these reactions, producing hydrogen sulfide (H_2S), which aggressively attacks CH and C–S–H [13].

Despite these insights, experimental investigations [5,12,14–20] are scarce to validate the potential reactions from the thermodynamic models at different conditions. Some experimental studies are conducted without control measurements using inert gases, making it difficult to distinguish effects caused by hydrogen. Elevated temperature and pressure, as well as changes in humidity, affect the material properties and need to be considered carefully. Additionally, due to the complex microstructure of the hardened cement paste, test preparation steps (e.g., drying of the samples) can significantly affect the integrity of the samples and make a comparison before and after the exposure difficult. Especially the permeability as a crucial parameter for well integrity can easily be compromised by incorrect preparation steps. Since alterations can develop very slowly, the mineral composition of the sample surface can indicate changes before they become apparent through a change in mechanical behaviour or permeability and porosity.

Another challenge for underground hydrogen storage is that compared to natural gas, hydrogen has higher mobility due to its low molecular mass, low viscosity, and low density [2,21], increasing the risk of leakage through microcracks and the material (permeability and diffusion pathways). This demands stricter requirements for the gas-tightness and integrity of the cemented boreholes. Additionally, UHS may involve more frequent injection and withdrawal cycles (up to daily or weekly basis), unlike the typical seasonal cycle for natural gas. This subjects the cement to greater thermal and mechanical stress, potentially accelerating degradation [22].

To enhance performance, polymer-modified (latex-modified) cements have been used since 1950s. These systems enhance slurry properties (e.g., fluid-loss control and rheology) and hardened cement characteristics (e.g., reduced permeability, improved bonding strength to the steel casing, flexibility, chemical resistance and reduced shrinkage). Their performance depends on polymer type, amount, and characteristics. Monomers, including vinyl acetate, vinyl chloride, acrylics, acrylonitrile, ethylene, styrene and butadiene can be used in the production of polymer-modified cement systems [6]. The amount of (dry) polymers typically used is limited to a maximum of about 5 wt% of the cement (bwoc). Existing studies focus on specific applications but rarely assess overall physical and mechanical properties. So far, for UHS, there are no investigations into potential interactions of hardened polymer-modified cement pastes with hydrogen.

This study addresses these research gaps, by experimentally investigating interactions between hydrogen and both conventional and polymer-modified hardened cement pastes. Experiments are conducted under 50 °C and 100 bar, simulating near-wellbore conditions. The study evaluates a unique combination of microstructural, mechanical, and physical changes to assess material integrity and suitability for long-term UHS. To separate the effects of individual parameters different conditions have been chosen, providing a deep insight into the individual details.

2. Materials and methods

2.1. Materials

In this study a high-sulfate resisting API Class G Grade HSR has been used, which contains theoretically no C_3A. The cement was provided by Dyckerhoff GmbH in Lengerich, Germany, and its chemical composition is given in Table 1. The water-to-cement ratio (w/c) was set to 0.44 according to API SPEC 10 A [4].

To examinate polymer-modified hardened cement paste typical representatives of polymer dispersion for cementitious materials were used:

- Polymer 1 (P1): Styrene-Acrylic Ester (SAE)
- Polymer 2 (P2): Styrene-Butadiene (SB)
- Polymer 3 (P3): Ethylene Vinyl Acetate (EVA)

Four different material mixtures were examined: One pure cement slurry as reference (REF) and three polymer-modified cement slurries. The water content of the polymer dispersions (ranging from 50 % to 67 %) was considered for the w/c ratio and the polymer to cement content (p/c ratio) was calculated by the solid content of the polymers.

Due to the effect of the polymer dispersions on the rheological properties and hardening process of the cement paste, additives were necessary to produce practical slurry mixtures (Table 2). The polymer dispersions generally used in the construction sector are adapted to the highly alkaline conditions in the cement slurry but not specifically developed for wellbore cementation. Thus, a high percentage of polymers with 20 wt.-% of the cement content was used to detect potential reactions with the composite material, which would not be detectable at a value commonly used in practice (e.g. up to 5 wt%). Although such mixtures can exhibit weaknesses in terms of material behaviour (mechanical, microstructural, etc.) and therefore do not necessarily represent a practical mixture used in the field.

The cement slurries were mixed according to the API Spec 10A [4]. For the polymer-modified cements, all liquid components were mixed first and then the dry components were added with the same mixing procedure. For each material, three prisms (40 x 40 × 160 mm^3) were cast, demoulded after 1 day (REF) and 3 days due to slower hydration (P1, P2, P3) and cured in deionised water at 20 °C. The water, saturated with the soluble minerals of the hardened cement paste, was subsequently used as storage water to avoid the dissolution of minerals. After one month, 60 drill cores (15 for each material) with a diameter and length of 25 mm were extracted from the prisms and the surfaces were parallel-polished. The full list of samples including test results are given in the SM-Table S2.

2.2. Experimental methods

Three corrosion-resistant batch reactors were used for the batch experiments, as shown in Fig. 1, based on [23]. The batch reactors are composed of an inner PEEK isolator housed in a stainless-steel autoclave.

To ensure comparability and separately compare the potential effects of hydrogen exposure from other variables, all cement samples were cured and altered/stored under identical timelines, as shown in Fig. 2. This approach accounts for changes in cement properties due to curing time and exposure, allowing observed differences to be attributed specifically to hydrogen interaction. Details to the experimental methods are given in SM.

One day before the alteration experiments, the mass, the dimensions

Table 1
Chemical composition of Class G HSR Cement used in the experiments, oxides determined by XRF (WDX (S8, Bruker), Sulfate determined by Carbon–Sulfur-Analyzer (calculated as max. SO_3 using molar masses) and LOI according to standard DIN EN 196–2:2013–10.

Na_2O	MgO	Al_2O_3	SiO_2	P_2O_5	K_2O	CaO	TiO_2	MnO	Fe_2O_3	SO_3	LOI
0.11	1.05	4.67	20.24	0.11	0.73	60.50	0.28	0.13	6.07	2.57	1.67

Table 2
The compositions of the slurry mixtures.

	REF	P1 (SAE)	P2 (SB)	P3 (EVA)
Water/cement - ratio (w/c)	0.44	0.44	0.44	0.44
Polymer/cement - ratio (p/c)	/	0.20	0.20	0.20
Stabilizer	/	0.40 wt% of c	0.48 wt% of c	/
Accelerator (calcium nitrate – tetrahydrate based)	/	2.00 wt% of c	2.00 wt% of c	/
Dispersant (PCE powder)	/	/	/	0.07 wt% of c
Anti-foam agent (fatty acid ester)	/	/	/	2.00 wt% of c

and the dynamic Young's modulus of each sample were measured and pictures under the microscope with a magnification of up to 200 were taken to detect potential cracks. Additionally, some of the samples were tested without any further alteration in preliminary tests. In total 39 of 60 samples were placed in different conditions for 4 weeks:

- H_2 Autoclave at 50 °C, 100 bar and 100 % RH (H_2)
- He Autoclave at 50 °C, 100 bar, 100 % RH (He)
- Air filled Duran glass bottle at 50 °C, 100 % RH (50 °C)
- Water bath at 50 °C (50 °C W)
- Water bath at 20 °C (20 °C W)

Due to the low solubility of hydrogen ($16x10^{-4}$ g/L in water at standard conditions) [13], minimal reactivity of the hardened cement paste with hydrogen over a few weeks is expected, when the samples are submerged in water. Since water can also act as a catalyst and subsurface conditions between casing and formation are typically water-saturated, tests were conducted under saturated conditions (100 % RH), maintained by placing small water-filled tubes inside the batch reactors. After pressurization, the reactors were sealed, and pressure was monitored (Fig. 3).

After 4 weeks of exposure, the samples were immediately analysed for mass, dimensions, dynamic Young's modulus and surface condition via optical microscopy. They were then dried in a climate room (20 °C, 65 % RH) for 14 days, with measurements to monitor the drying process.

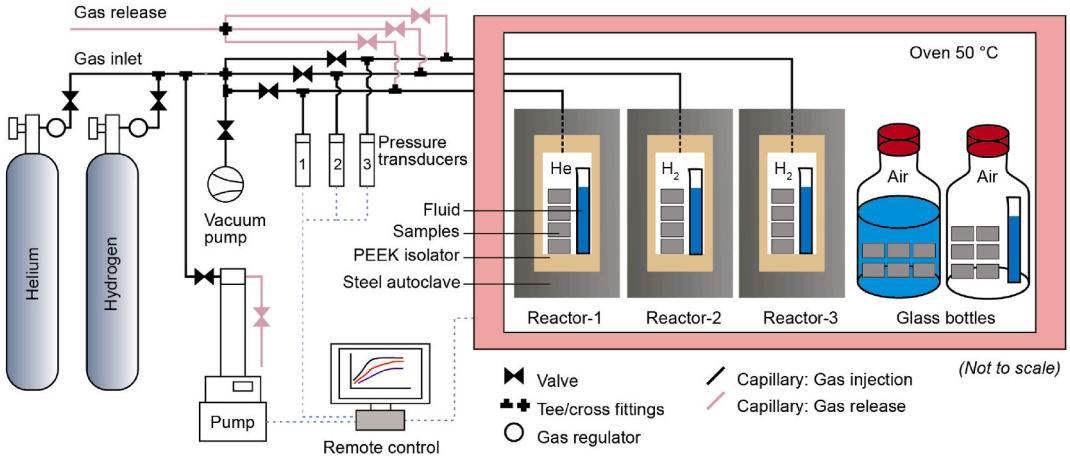

Fig. 1. *Schematic representation of the static batch reactors used for hydrogen alteration experiments, including three reactors connected in parallel with hydrogen and helium cylinders, and two 0.5 L Duran glass bottles sealed with a rubber stopper (modified from [23]).*

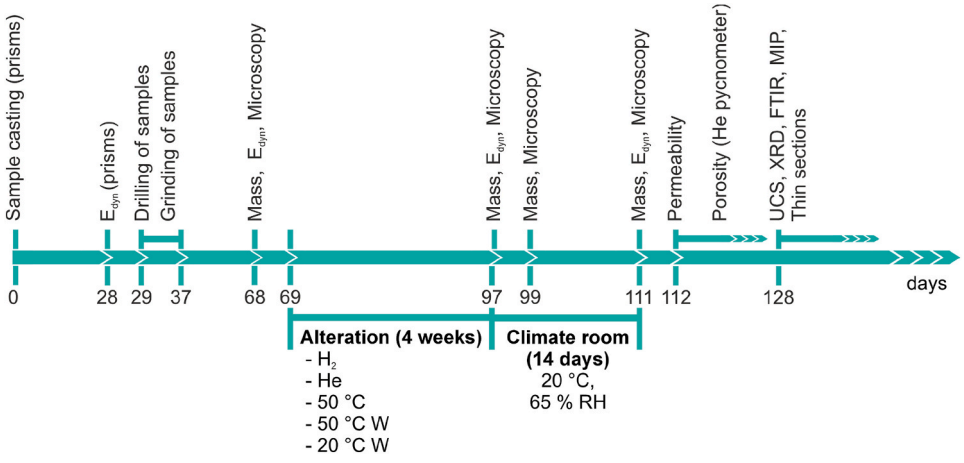

Fig. 2. Timeline of the experiments in days.

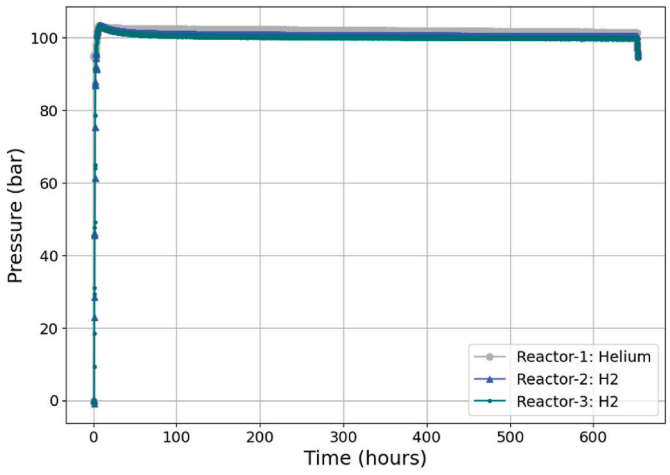

Fig. 3. Internal pressures of the 3 reactors throughout the experiments.

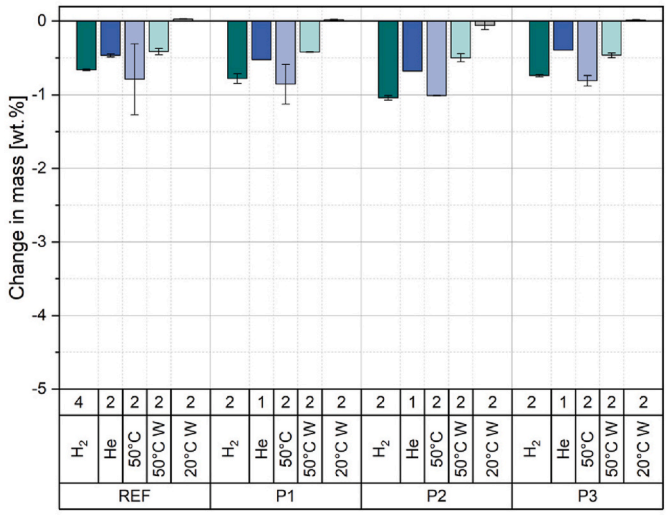

Fig. 4. Change in mass [wt. %] before and after 4 weeks of exposure in different conditions. Columns at the bottom: number of tested samples (1st), condition (2nd) and material (3rd).

Afterwards, the samples were placed in small plastic bags to prevent further changes in the water content. Permeability was tested after day 15 and the porosity was measured with a helium pycnometer in the following days due to the long duration of the test. Afterwards, the samples were tested for unconfined compressive strength. For further analysis, some material was crushed for Mercury Intrusion Porosimetry (MIP), while the surface of the samples was extracted and ground to powder with a mortar and pestle, sieved to 63 µm and stored in a desiccator for X-ray diffraction (XRD) and Fourier Transform Infrared Spectroscopy (FTIR) measurements.

3. Results

3.1. Pressure monitoring during alteration

The internal pressures of the autoclaves were continuously recorded throughout the experiment (Fig. 3). Pressurization and heating were carried out, reaching final pressure of approximately 103 bar. Within the first two days, the initial pressures slightly dropped and stabilised nearly to a constant level due to approaching thermodynamic equilibrium. Over the 4-week exposure period, the autoclaves exhibited a gradual pressure loss of approximately 1 bar, indicating a sufficient gas tightness.

3.2. Mass change and optical microscopy

All the samples investigated in this study exhibited negative mass change under elevated temperature conditions (Fig. 4). The samples submerged in water at 20 °C (no condition change) showed constant mass with minimal variation. H_2-exposed samples displayed lower mass compared to He-exposed samples, with increased influence on the polymer-modified samples. Variability in results was lower in autoclave and water bath setups than in the Duran glass bottle filled with air.

No colour changes were observed after exposure. However, white surface precipitates—presumed to be portlandite (CH)—were found on samples from both autoclaves and glass flasks, consistent with known behaviour during prolonged water storage. Surface inspection under optical microscopy (up to 200 × magnification) revealed crack formation, with representative images provided in the SM-Fig. S6–S9.

Prior to exposure, REF, P2 and P3 samples showed no detectable surface cracks, while all P1 samples exhibited cracks with crack apertures up to 11 µm (SM-Fig. S7). Post exposure, REF and P3 samples remained intact, whereas P2 samples developed cracks under all conditions (up to 9 µm). After two days of drying (20 °C, 65 % RH), REF and P3 samples remained crack-free. In contrast, P1 samples showed increased crack apertures up to 30 µm, with one crack up to 88 µm. P2 samples showed apertures up to 14 µm, with one crack up to 48 µm. After 14 days of drying, the REF and P3 samples remained largely intact, except for REF BK 1 (H_2, 50 °C, 100 bar) and REF BK 11 (20 °C), which developed one crack with 1 µm and 4 µm. P1 samples showed crack apertures ranging from 1 µm to 8 µm, while P2 samples ranged from 5 µm to 22 µm.

3.3. Dynamic Young's modulus

The dynamic Young's modulus (E_{dyn}) of the cement prisms were measured 28 days after casting (Table 3). The polymer modified cements showed a reduction of E_{dyn} between 39.2 % and 49.6 % in comparison to the reference material (REF).

E_{dyn} was measured before and after the 4 weeks in different conditions, and the changes in E_{dyn} are shown in Fig. 5. For the reference material (REF), a slight increase of E_{dyn} was observed at 20 °C in the water bath, attributed to continued hydration. A similar trend was seen at 50 °C. The exposure to H_2 lead to a minor reduction in average E_{dyn} with both slightly positive and negative single values. The He-exposure lead to an increase, though the two samples showed differing values (+4,52 and + 0,95 %).

For the polymer samples (P2 and P3), the increase of E_{dyn} at 20 °C in the water bath was more pronounced than for the REF samples, while P1 remained at a nearly constant level. With increasing pressure and temperature, E_{dyn} of polymer samples was reduced, with P2 being most affected with approx. 13 % for 50 °C and 100 bar.

3.4. Permeability and porosity

The intact REF and P3 samples exhibited permeabilities below the instrumental detection limit ($k < 0.0001$ mD or 9.9×10^{-20} m^2). Measurable permeability was only observed in samples with visible cracks, though values remained low, averaging around 0.03 mD. The highest recorded permeability was 0.28 mD for sample P2 BK 10.

Regarding effective porosity (Fig. 6), REF samples showed similar values to those stored at elevated temperatures (H_2, He, 50 °C and 50 °C W), while samples at 20 °C had lower effective porosity. Polymer-modified samples displayed significant variation depending on temperature and humidity. For P1 and P2 H_2-exposure led to higher effective porosity than He-exposure, while for P3 the value remained comparable. Regarding the testing procedure, only the accessible porosity was measured, pores filled with water or isolated ones can

Table 3
Dynamic Young's modulus (E_{dyn}) of the 28-day-old prisms.

	REF	P1	P2	P3
E_{dyn} [MPa]	20072, 20051, 19965 (20029 on average)	12254, 12260, 12027 (12180 on average)	11743, 11709, 11700 (11717 on average)	10045, 10140, 10073 (10086 on average)

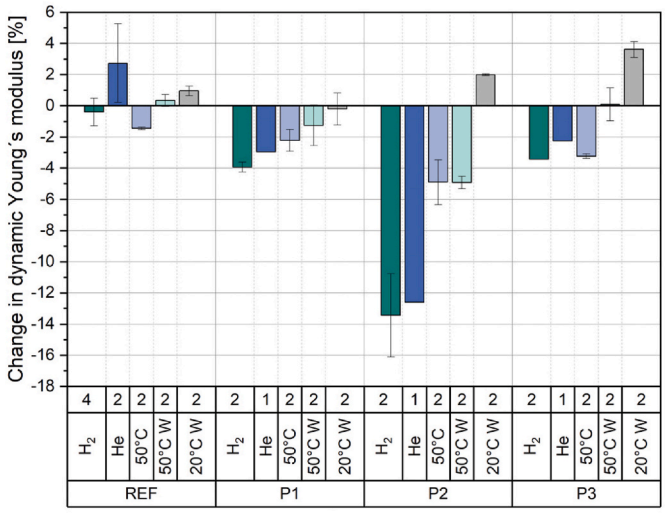

Fig. 5. Average change in the dynamic Young's modulus before and after 4 weeks in different conditions. Columns at the bottom: number of tested samples (1st), condition (2nd) and material (3rd).

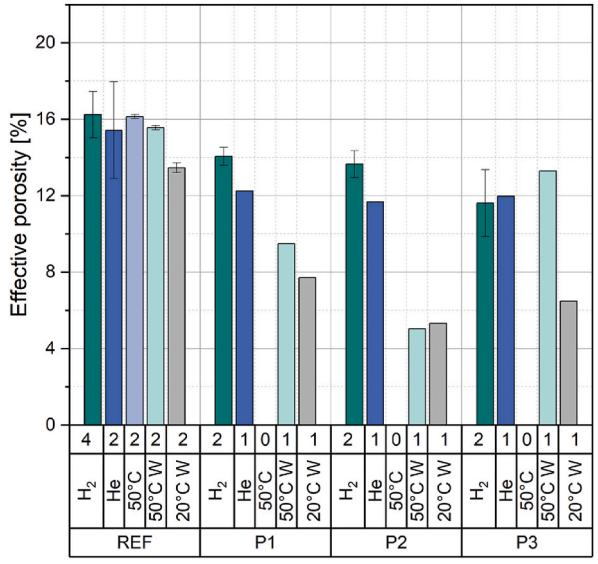

Fig. 6. Porosity (He-pycnometer) after 14 days of drying (20 °C, 65 % RH), measured at 20 °C. Columns at the bottom: number of tested samples (1st), condition (2nd) and material (3rd).

highly affect the measured values. Overall, porosity varied considerably between samples. After 14 days, the tested temperature over 4 weeks showed an influence on the effective porosity, which varied depending on the material used.

In addition to the measurements with the He-pycnometer, Mercury Intrusion Porosimetry (MIP) measurements were carried out for all H_2- and He-exposed samples. The results are given in Fig. 7 and Table 4.

Depending on the polymer modification (P1, P2, P3), the peaks of the pore entry radius differed and were generally smaller than that those of the REF. In contrast, the incremental volume dV/dlog(r) for a pore entry radius >1 µm of P1, P2 and P3 samples were higher, showing higher coarse porosity.

Considering the natural scattering of the material, no apparent change due to hydrogen was detectable for any of the materials (REF, P1, P2, P3), neither in the total percentage, nor in the finer (<1 µm) nor coarser (1 µm–200 µm) porosity.

3.5. Compressive strength

As shown in Fig. 8, the curing conditions had limited effect on the compressive strength of each mix, as few variations can be seen for the same material. REF samples showed reduced strength under H_2- compared to He-exposure, though results had high standard deviation. Additionally, P1 samples cured at 20 °C in a water bath showed lower compressive strength compared to the other conditions.

3.6. X-ray powder diffraction (XRD)

The XRD patterns of all H_2 and He exposed samples (Fig. 9) show that the major crystalline phase was portlandite (CH) and small contents of ettringite and quartz were detected. Even after more than 4 months, residual clinker phases in the form of belite (C_2S), alite (C_3S), brownmillerite (C_4AF) were identified.

Gypsum peaks were absent, likely due to complete consumption over time. Although calcite formation was expected after 14 days of drying, it was not detected. Some of the calcite peaks overlap with C_2S and C_3S peaks, complicating precise identification. The broad hump beneath the diffraction peaks (background) indicates the amorphous phases that cannot be considered with XRD in detail, like C–S–H [24], Fe-containing hydrates [25] and the polymer-content. Polymer-modified samples showed similar patterns to REF samples, but with lower peak intensities due to partial cement replacement.

Qualitative comparison of H_2- and He-exposed samples (SM-Fig. S12 and S13) revealed the most notable changes in CH peaks, while C_2S and C_3S varied slightly without a clear trend. No changes were observed for C_4AF and ettringite, and no new crystalline phases were detected, despite measurement uncertainties. Polymer-modified cements behaved similarly, indicating no interaction or alteration of crystalline phases in the hardened paste.

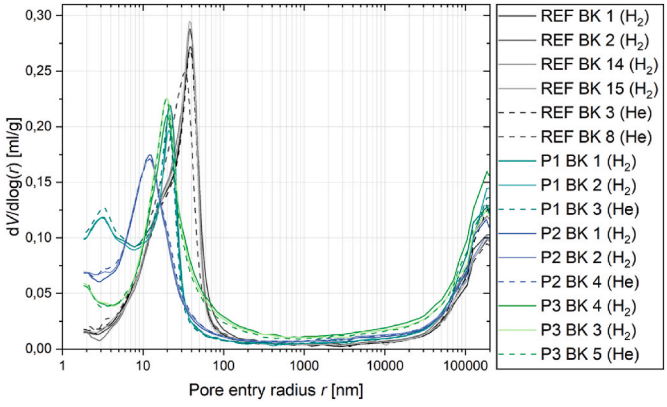

Fig. 7. Pore size distribution of all H_2- and He-exposed samples (50 °C, 100 bar) determined by Mercury Intrusion Porosimetry (MIP).

Table 4
Cumulative MIP pore volumes of all H_2- and He-exposed samples (50 °C, 100 bar).

Porosity [%]	Sample														
	REF						P1			P2			P3		
	BK 1 (H_2)	BK 2 (H_2)	BK 14 (H_2)	BK 15 (H_2)	BK 3 (He)	BK 8 (He)	BK 1 (H_2)	BK 2 (H_2)	BK 3 (He)	BK 1 (H_2)	BK 2 (H_2)	BK 4 (He)	BK 3 (H_2)	BK 4 (H_2)	BK 5 (He)
Total	31.6	32.6	33.0	32.1	31.5	32.1	30.4	30.5	30.5	28.1	28.0	28.8	31.6	32.5	31.0
Coarse (>1 µm)	7.5	8.1	9.3	7.9	8.7	7.5	9.4	9.2	9.2	9.3	8.7	9.4	10.7	12.3	10.8
Fine (<1 µm)	24.1	24.5	23.7	24.2	22.8	24.6	21.0	21.2	21.3	18.8	19.3	19.4	21.0	20.2	20.2

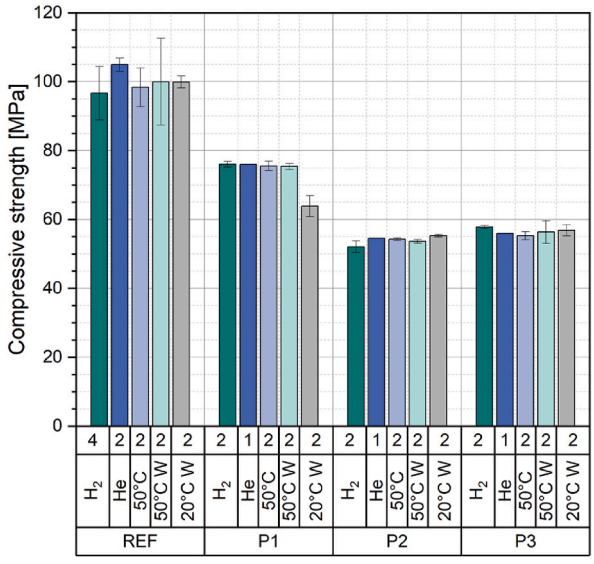

Fig. 8. Compressive strength of all samples after 128 or 164 days. Columns at the bottom: number of tested samples (1st), condition (2nd) and material (3rd).

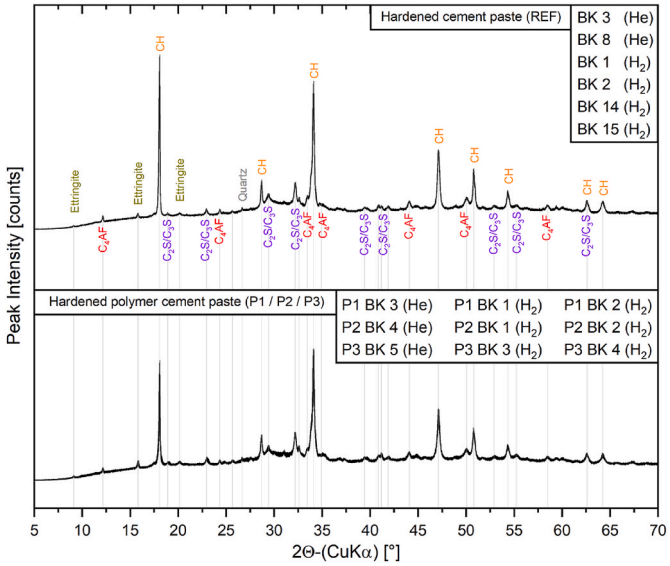

Fig. 9. Overlapping X-Ray powder diffraction pattern of all H_2- and He-exposed samples (50 °C, 100 bar) and the qualitative identification of the crystalline phases, measured at 20 °C.

3.7. Fourier transform infrared spectroscopy (FT-IR)

Fig. 10 shows the IR spectra of the investigated samples in H_2 and He conditions (50 °C, 100 bar for 4 weeks). The IR spectra revealed distinct absorption bands that enabled a clear differentiation between the samples. The focus was placed on the identification of characteristic vibrational modes corresponding to functional groups such as ester (C═O, C–O), carboxylic acid (C═O, C–O), hydroxyl (O–H), aromatic rings (C–H), Methyl (C–H), carbonate (CO_3^{2-}), sulfate (S–O), and silicate (Si–O) moieties. Identified peaks in the IR spectra were summarized in Table 5.

The main hydrated phases of the cement were identified at 3641 cm^{-1} for CH and several peaks between 1100 and 900 cm^{-1} with main peak at 959 cm^{-1}. The broad band with a peak at.

3407 cm^{-1} were assigned to free water, bound and adsorbed water of C–S–H, AFm and AFt phases as well as polymers. Carbonate phases were identified at 1470, 1421 and 873 cm^{-1}. Peaks between 2400 and 1950 cm^{-1} are attributed to atmospheric influences and therefore not further investigated. AFt and AFm phases show complex spectra as their peaks overlap with the functional groups of other hydrated phases. Therefore, AFt and AFm phases could not easily be identified. Only ettringite was identified separately as the dominant representative of the AFt phases with a peak at 1115 cm^{-1}.

A fingerprint for the styrene-containing polymers SAE and SB (P1 and P2) provided the presence of aromatic rings at 3028 cm^{-1} and 698 cm^{-1}. In the P1 samples carboxylic acid bands at 1731 and 1160 cm^{-1} were identified. For the P3 samples (EVA) ester-related peaks around 1736 cm^{-1} and 1242 cm^{-1} indicate unreacted methacrylate groups. Additionally, methyl was identified in all polymer samples (P1, P2, P3) with peaks at approx. 2920 and 2850 cm^{-1}. It is suggested that some of the REF-samples were contaminated with the latter (peaks at 2917 and 2851 cm^{-1}) due to the same storage in the autoclave system and saturated storage water.

3.8. Thin sections

Thin sections of one sample per material exposed to H_2 and He were examined with an optical microscope (shown in Fig. 12). Carbonation depth varied due to post-exposure storage in the climate room. Surface alterations from drilling and grinding were also visible. The carbonation depth is most pronounced in the REF (up to 175 µm) and P1 samples (up to 90 µm), moderate in P2 samples (up to 54 µm), and not detectable in P3 samples. No significant differences were observed between H_2 and He exposure conditions.

4. Discussion

4.1. Microstructure and potential reactivity with hydrogen

Thermodynamic modelling suggests that hydrogen exposure can induce several changes in the mineralogical phases of the hardened cement paste [9–12], including reduction of sulfate phases to sulfite and transformation of iron- and aluminium-bearing phases (C_4AF, C_3A, ettringite, and hematite) into new phases (e.g., C_3AH_6 and maghemite [10]). Calcite dissolution is also possible. While polymers are not expected to react strongly with hydrogen, they may influence composite

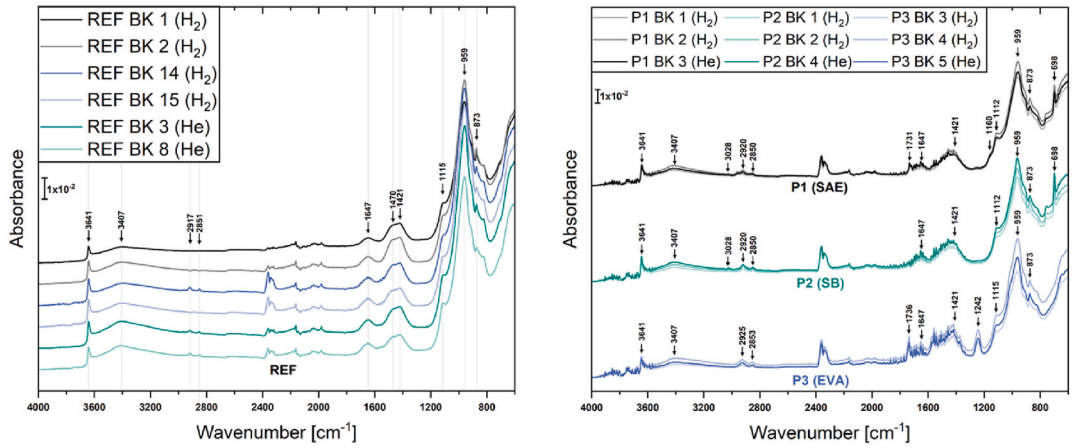

Fig. 10. *IR spectra (4000 – 600 cm^{-1}) with identified peaks of all H_2- and He-exposed samples* (50 °C, 100 bar), *on the left: REF samples and on the right: polymer samples (P1, P2, P3).*

Table 5
Identified functional groups in IR spectra with corresponding IR mode and wavenumber as well as assignment to literature sources with ν: stretching vibration, ν_{asym}: asymmetric stretching vibration and δ: bending/out of plane vibration.

Functional group	IR-mode	Wavenumber [cm^{-1}]	Literature
Carbonic acid	ν (C═O), ν (C–O)	1731, 1160	[26]
Aromatic ring	ν (C–H), δ (C–H)	3028, 698	[27,28]
Ester	ν (C═O), ν (C–O)	1736, 1242	[26,29–31]
Methyl	ν_{asym} (C-H$_x$)	2920, 2850	[29–31]
Calcium-hydroxide (CH)	ν (O–H)	3641	[29,31–35]
Carbonate	ν_{asym} (CO_3^{2-}), ν_{asym} (CO_3^{2-}), δ (CO_3^{2-})	1470, 1421, 873	[31,32,36]
Water	ν (O–H), δ (O–H)	Broad band with peak at 3407, 1647	[29,31,32, 35,36].
Calcium-silcate-hydrates (C–S–H)	ν (Si–O)	several peaks between 1100 and 900 with main peak at 959	[29,31–36]
Sulfate	ν (S–O)	1115	[26,31,33].

properties.

C_4AF shows a very slow hydration rate and is commonly found in hydrated cements over a long period of time [12,17,37]. Its potential reaction with H_2 could affect porosity, permeability, and mechanical strength, impacting well integrity. However, XRD analysis shows stable peaks for C_4AF and ettringite (Fig. 9), with no evidence of new iron- or aluminium phases like hematite, magnetite, mackinawite, C_3A or hydrogarnet (C_3AH_6) or sulfate-containing phases like calcium monosulfoaluminate (AFm). In alignment with the XRD measurements the IR spectra show no changes comparing H_2- and He-exposed samples, indicating no new mineral phases due to hydrogen exposure.

The main hydration products, CH and C–S–H, are most challenging to evaluate for possible alterations, because the X-ray absorption of CH is dependent on the crystalline orientation [24]. From the FT-IR, a unique peak for CH at 3641 cm^{-1} can be used, but it varies across samples. C–S–H, being an amorphous structure, is not detectable by XRD and presents overlapping FT-IR peaks (1100 - 900 cm^{-1}) (Fig. 10). For the main hydration products no systematic changes were observed, aligning with thermodynamic modelling results [9–12] that no reaction occur in the absence of CO_2. These findings are consistent across both reference and polymer-modified samples. Even at higher temperatures, the quantitative XRD results carried out by Iorio et al. [12] (90 °C, 150 bar, saturated sample during exposure) and the qualitative XRD results of Corina et al. [17] (80 °C, 200 bar, submerged in brine) show no systematic changes. Porewater chemistry performed by Aftab et al. [5] support the results, where no significant changes between hydrogen and nitrogen exposed samples were detected.

Contrary to thermodynamic expectations, no detectable alterations of the potential sensitive mineral phases occurred under the tested conditions (50 °C, 100 bar). Stable reactor pressures (Fig. 3) support the absence of density-changing reactions with H_2 according to Le Chatelier's principle. Microscopy of thin sections (Fig. 12) revealed no near-surface differences between H_2- and He-exposed samples, aside from minor carbonation from post-exposure drying.

For polymer-modified hardened cement paste, no prior H_2 exposure studies exist. While polymers interact physio-chemically with cement, but in the long term, hydration products (CH, C–S–H) remain largely unaffected by SAE, SB, or EVA modification, as shown in XRD and FT-IR data (Figs. 9 and 10). For the polymer content the IR spectral data allowed the unambiguous assignment of the polymer identities and their respective reactivities toward hydrogen and the cement matrix. Since some parts of the polymers are not completely saturated with hydrogen (SM- Fig. S11), alterations could occur.

Comparison of H_2- and He-exposed samples (Figs. 10 and 11) revealed no consistent changes due to hydrogen exposure, expect for a minor changes for P2 samples (SB polymer) in the peak at 698 cm^1 assigned to the aromatic rings. However, for P1 with the same identified peak no changes are observed. Since no potential reaction of the aromatic rings with hydrogen is to be expected, it is assumed that this is only a variation in the measurement results.

Besides the potential reaction with hydrogen, the stability of the polymers also depends on the temperature and the alkalinity [29, 38–40]. IR spectra indicate hydrolysis in relation to the cement matrix. P1 samples (SAE) showed carboxylic acid bands at 1731 and 1160 cm^{-1}, while P2 (SB) exhibited loss of C═C double bonds, with no peaks between 1700 and 1600 cm^{-1}. Comparing the H_2-exposure with the other conditions (50 °C, 50 °C W, 20 °C W) showed no significant spectral differences. It's suggested that hydrolysis is primarily driven by alkaline conditions. However, these effects do not necessarily impair mechanical performance.

A potential reaction of calcite with hydrogen was not examined experimentally in this study. However, discrepancies persist in the literature regarding the reaction of calcite with hydrogen. Thermodynamic modelling predicts calcite dissolution with methane production at 95 °C and 100 bar [10]. However, experimental studies by Gelencsér et al. [41] with natural calcite at 105 °C and 100 bar and by Cheng et al. [23] on calcite-bearing sandstones at 100 °C and 150 bar found no reaction.

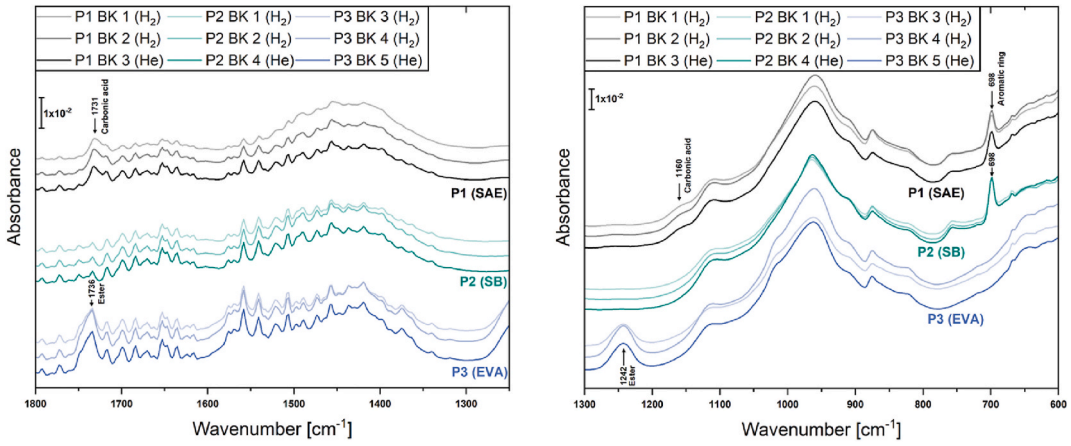

Fig. 11. IR spectra between 1800 and 1250 cm^{-1} (left) and 1300 – 600 cm^{-1} (right) with identified peaks associated with the polymers of all H_2- and He-exposed polymer samples (50 °C, 100 bar).

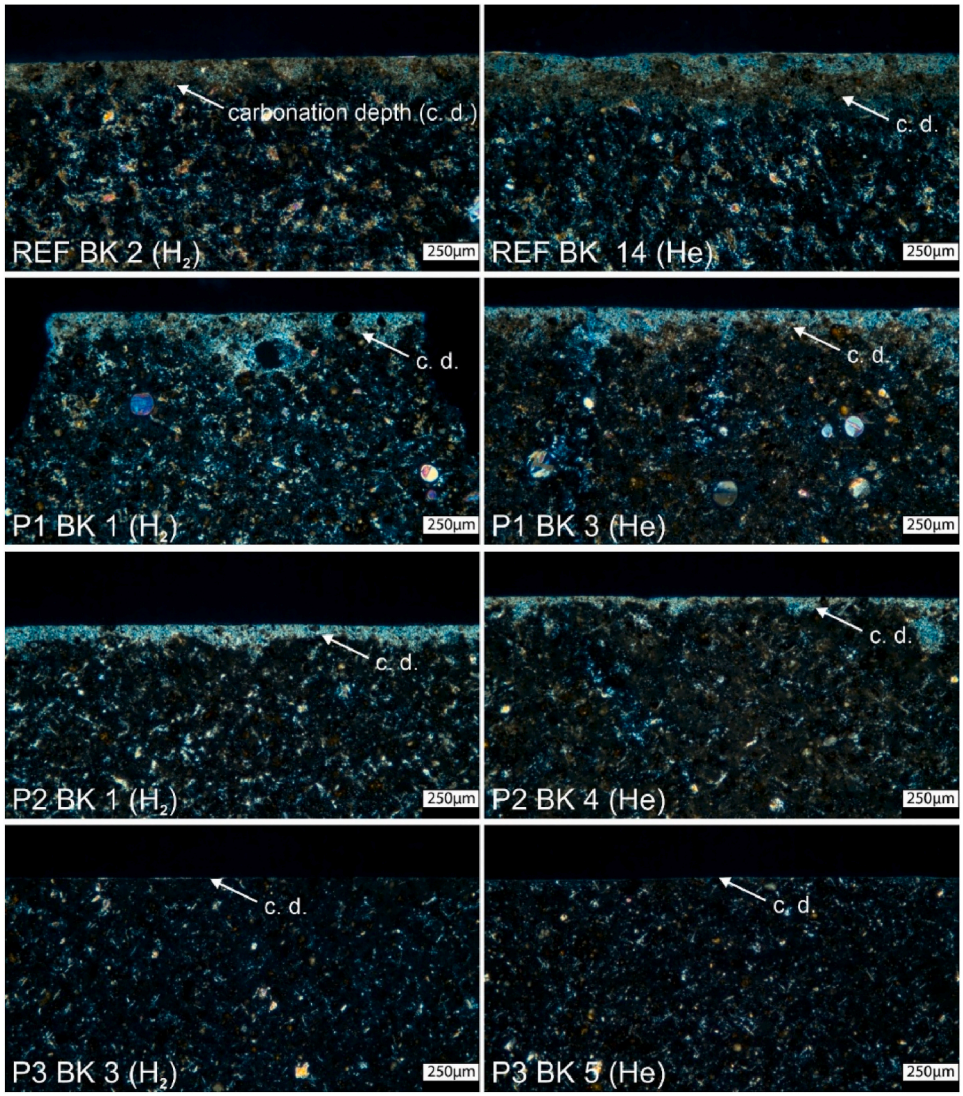

Fig. 12. Thin Section images of H_2- and He-exposed samples under an optical microscope with crossed-polarized light (XPL). Lighter areas show carbonation of the surface due to drying in the climate room.

4.2. Alteration of mechanical and physical properties by hydrogen

For long-term and safe storage, the possible changes in mechanical and physical properties are of crucial importance and are discussed in the following sections. However, the literature presents inconsistent findings on this topic, which will be further examined in the following sections.

4.2.1. Compressive strength and stiffness

Hardened cement paste is a brittle material and shows a significant natural variability in compressive strength, which can be misleading with a low number of samples. Additionally, the results are strongly dependent on the storage and testing conditions, such as moisture content.

REF samples exposed to H_2 showed a 7.9 % reduction in compressive strength compared to He, but this lies within the standard deviation (Fig. 8). Especially one outlier (86.2 MPa) notably lowered the average to 96.7 MPa. Literature also reports variability: Cracolici et al. [14] reported ~ 10 % strength reduction after exposure to both H_2 and N_2 compared to samples tested before exposure. Iorio et al. [12] observed decreased strength with pure cement but an increase with cement blended with 35 % silica flour, with a slightly higher compressive strength after H_2- than N_2-exposure. Corina et al. [17] observed that H_2-exposed samples had the lowest compressive strength compared to N_2 and non-exposed samples. The discrepancies may result from higher testing temperatures and pressures (80 –90 °C, 150–200 bar) than those used in this study (50 °C, 100 bar). Strength retrogression is unlikely below 110 °C [6], but rapid changes in temperature, humidity and pressure may result in excessive internal stress, leading to the formation of microcracks and reducing the compressive strength.

The H_2-exposed REF samples also show a slight reduction in E_{dyn} (approx. 3 % but with high variation, shown in Fig. 5) and mass (approx. 0.2 %, shown in Fig. 4), along with slightly increased effective porosity compared to the He-exposed ones (Fig. 6). Nevertheless, H_2-exposed samples remain comparable to those stored at 50 °C, indicating no noticeable changes due to the presence of hydrogen. Minor moisture loss during handling may explain the observed trends. Al-Yaseri et al. [16] reported increasing E_{dyn} after H_2-exposure, possibly due to continued hydration, though no inert gas control was used.

Polymer-modified samples (P1, P2, P3) showed no consistent strength reduction from H_2 exposure. All polymer samples exhibited ~0.2 % mass loss and Edyn reductions of 2–4 % (P1, P3) and 12–14 % (P2) under elevated temperature and pressure. For P1 and P3, this likely reflects thermoplastic behaviour. The temperature and pressure increase may allow the polymer to adapt to the changed conditions. P2 showed insufficient stability, discussed further in Section 4.3.

4.2.2. Permeability and porosity

Measured permeability was below the instrumental detection limits, preventing a direct comparison between H_2- and He-exposed samples. However, with a value below $k < 0.0001$ mD ($9.9 \cdot 10^{-20}$ m^2), a sufficient gas tightness of the cement can be assumed (section 3.4). The results are consistent with previous studies performed by Cracolici et al. [14] and Iorio et al. [12], which also reported stable permeability near the lower detection threshold. Corina et al. [17] reported permeability tests observing only minor permeability increases after 2–14 months of H_2 exposure, comparable to CH_4 and N_2.

In contrast, Shi et al. [19] observed a significant increase in permeability of 62.5 %, while the porosity decreased slightly by 0.2 %. Fernandez et al. [15] also showed an increase in permeability up to 70 % depending on the H_2 exposure time. These discrepancies likely result from sample drying before testing or exposure [15], and microcrack formation. Cementitious materials are highly sensitive to drying and fast pressure changes, especially when pores are not completely saturated.

This is underlined by crack observation in this study (section 3.2) and reported observations in the literature. The test procedure in this study was developed to prevent cracking of the REF samples in preliminary tests to ensure the validity of the measurements. However, P1 and P2 samples seem to be more sensitive and developed cracks, leading to increased permeability (section 3.4). Furthermore, salt precipitation can also affect permeability and porosity, as noted by Boersheim et al. [20].

Effective porosity measurements using He-pycnometry are affected by residual moisture. Without complete drying, moisture content remains unknown, but full drying risks damaging the samples. The 14-day climate room storage was insufficient for fully drying, as confirmed by tested backup samples and MIP results (Fig. 6 and Table 4). Moisture retention varies by material, so He-pycnometer results are only valid for samples with identical mix design and storage conditions. MIP data showed similar porosity for H_2- and He-exposed samples not affected by moisture variation, with no significant changes beyond natural variability.

Overall, this study emphasizes that sample preparation and the selected boundary conditions are critical for reliable porosity and permeability measurements with hardened cement paste samples. These factors likely explain the large variability reported in previous studies [15,19], where inconsistent results may may stem from handling and drying procedures.

4.3. Implications for underground hydrogen storage

This study applied a broad range of methods to assess potential material changes due to H_2 exposure. At 50 °C and 100 bar, no significant microstructural alterations in hydration phases or polymer bonding were observed. Minor changes in mechanical and physical properties varied by material but given the number of samples and natural variability, statistical reliability is limited. However, comparing the whole set of methods and tested conditions no systematic reactivity of the investigated materials with H_2 was observed and therefore, no significant risk during UHS within the investigated conditions are suggested.

In addition to the potential alteration of hardened cement paste, increased requirements due to higher cyclic loading and the greater gas mobility of hydrogen compared to natural gas remain. Polymer modification can improve slurry and hardened paste properties, increasing flexibility, bonding strength, chemical resistance, while decreasing permeability, stiffness, and compressive strength [6,29,42]. As Cement sheath failure is more influenced by the tensile strength-to-Young's modulus ratio, while compressive strength only plays a minor role [6] polymer modification could prevent stress-induced cracking and micro-annuli formation.

Since the polymer dispersions used were developed for applications in civil engineering rather than specifically for wellbore applications, their mechanical properties are only conditionally suitable. A high polymer content (20 wt% of cement) was used to highlight possible changes that would otherwise not be noticeable in quantities used typically in practice. As a result, some of the samples showed insufficient pressure and temperature stability, highlighting the need to differentiate influencing factors. However, the focus of this study was on the fundamental suitability of typical representative of polymers regarding their interaction with hydrogen. In this study no systematic alterations due to hydrogen were observed. The compressive strength, stiffness (E_{dyn}) and variability of those decrease with the increase in the polymer content, indicating a more flexible, homogeneous and less brittle material. The potential of polymer-modified cements slurries should therefore be investigated more in detail for long-term underground hydrogen storage.

5. Conclusions and outlook

Underground Hydrogen Storage (UHS) is a promising method to achieve a climate-friendly energy economy with renewable energy sources on a large scale. Thermodynamic modelling suggests potential reactivity of the cement mineral phases with hydrogen, potentially

compromising well integrity. Experimental data remain scarce and are often inconsistent, include variations in testing conditions and sample preparation or lack of control measurements. In this study, the microstructure in addition with physical and mechanical properties of both conventional and polymer-modified hardened cement pastes exposed to hydrogen were investigated. To examine the individual effects of gas type, temperature and pressure different conditions for the same timeline were chosen, ensuring a comprehensive comparison. The results are promising for the application of UHS, as no significant alterations under simulated underground conditions (50 °C, 100 bar over 4 weeks) were observed in wellbore and polymer-modified hardened cement pastes. Additionally, a polymer-modification could provide improved material properties to meet the increased requirements of UHS applications compared to natural gas storage. However, this study focused solely on abiotic reactivity with hydrogen in the absence of CO_2 and microbial activity. Future research should investigate more complex environments, including exposure to gas mixtures of H_2 and CO_2. Because CO_2 is also considered a potential cushion gas for hydrogen storage and naturally occurs in formation waters. Additionally, CO_2 content in brine can also be increased due to carbonate dissolution in reservoir or caprock formations. Its presence might trigger activation of some geochemical reactions between cement and CO_2-brine and potentially further facilitated by hydrogen.

CRediT authorship contribution statement

Sebastian Bruckschlögl: Writing – review & editing, Writing – original draft, Visualization, Validation, Resources, Project administration, Methodology, Investigation, Formal analysis, Data curation, Conceptualization. **Chaojie Cheng:** Writing – review & editing, Visualization, Validation, Supervision, Resources, Project administration, Methodology, Investigation, Conceptualization. **Peter Thissen:** Writing – review & editing, Supervision, Methodology, Formal analysis, Conceptualization. **Benjamin Busch:** Writing – review & editing, Supervision, Methodology, Conceptualization. **Christoph Hilgers:** Writing – review & editing, Supervision, Project administration, Funding acquisition. **Frank Dehn:** Writing – review & editing, Supervision, Project administration, Funding acquisition.

Conflict of interest

The authors declare that they have no known competing financial interests or personal relationships that could have appeared to influence the work reported in this paper.

Acknowledgement

This work is part of the SAMUH$_2$ project supported by the German Federal Ministry of Economic Affairs and Climate Action (BMWK) under grant no. 03EI3051A. The authors wish to thank Astrid Hirsch and Andreas Bogner for assistance with methodology and the XRD measurements, Martin von Dollen for thin section preparation, Vanessa Mercedes Kind for insightful discussions during the planning phase, Laura Rossi and Selina Schwarz for proof reading. We also like to thank Dyckerhoff GmbH for providing the Class G cement and the consulted companies providing the polymer dispersions and additives.

Appendix A. Supplementary data

Supplementary data to this article can be found online at https://doi.org/10.1016/j.ijhydene.2026.153578.

References

[1] Heinemann N, et al. Enabling large-scale hydrogen storage in porous media – the scientific challenges. Energy Environ Sci 2021;14(2):853–64. https://doi.org/10.1039/D0EE03536J.
[2] Miocic J, Heinemann N, Edlmann K, Scafidi J, Molaei F, Alcalde J. Underground hydrogen storage: a review, vol 528. Geological Society, London, Special Publications; 2023. p. 73–86. https://doi.org/10.1144/SP528-2022-88.
[3] Perera M. A review of underground hydrogen storage in depleted gas reservoirs: insights into various rock-fluid interaction mechanisms and their impact on the process integrity. Fuel 2023;334. https://doi.org/10.1016/j.fuel.2022.126677.
[4] API specification 10A: cements and materials for well cementing. 2019.
[5] Aftab A, et al. Geochemical integrity of wellbore cements during geological hydrogen storage. Environ Sci Technol Lett 2023;10(7):551–6. https://doi.org/10.1021/acs.estlett.3c00303.
[6] Nelson EB, Guillot D. Well cementing. second ed. 2006.
[7] Kutchko BG, Strazisar BR, Dzombak DA, Lowry GV, Thaulow N. Degradation of well cement by CO2 under geologic sequestration conditions. Environ Sci Technol 2007;41(13):4787–92. https://doi.org/10.1021/ES062828C.
[8] Carey JW, et al. Analysis and performance of oil well cement with 30 years of CO2 exposure from the SACROC unit, west Texas, USA. Int J Greenh Gas Control 2007;1(1):75–85. https://doi.org/10.1016/S1750-5836(06)00004-1.
[9] Jacquemet N, Chiquet P, Grauls A. Hydrogen reactivity with (1) a well cement-PHREEQC geochemical thermodynamics calculations. 1st geoscience & engineering in energy transition conference, vol 2020. European Association of Geoscientists & Engineers; 2020. p. 1–5. https://doi.org/10.3997/2214-4609.202021018. 1.
[10] Zeng L, et al. Thermodynamic modelling on wellbore cement integrity during underground hydrogen storage in depleted gas reservoirs. In: SPE Asia Pacific oil and gas conference and exhibition; 2022, D021S009R003. https://doi.org/10.2118/210639-MS. SPE.
[11] Sun G, Li B, Yang W, Guo J, Guo H. Analysis of energy consumption of the reduction of Fe2O3 by hydrogen and carbon monoxide mixtures. Energies 2020;13(8). https://doi.org/10.3390/en13081986. Art no. 1986.
[12] Iorio VS, et al. Cement to safeguard the wells integrity in underground hydrogen storage: an experimental investigation. Chemical Engineering Transactions 2022;96:307–12. https://doi.org/10.3303/CET2296052.
[13] Ugarte ER, Salehi S. A review on well integrity issues for underground hydrogen storage. J Energy Resour Technol 2022;144(4). https://doi.org/10.1115/1.4052626. Art no. 042001-1.
[14] Cracolici F, et al. Experimental investigation of cement compatibility in underground hydrogen storage in depleted reservoir. Bangkok, Thailand: International Petroleum Technology Conference; 2023. https://doi.org/10.2523/IPTC-22797-MS.
[15] Fernandez DM, Emadi H, Hussain A, Thiyagarajan SR, Ispas I, Watson M. Experimental investigation of the impact of short-term hydrogen exposure on cement sheath's mechanical and sealing integrity. Geoenergy Sci Eng 2025;251. https://doi.org/10.1016/j.geoen.2025.213885. Art no. 213885.
[16] Al-Yaseri A, Fatah A, Zeng L, Al-Ramadhan A, Sarmadivaleh M, Xie Q. On hydrogen-cement reaction: investigation on well integrity during underground hydrogen storage. Int J Hydrogen Energy 2023;48(91):35610–23. https://doi.org/10.1016/j.ijhydene.2023.05.304.
[17] Corina AN, Soustelle V, ter Heege J. Report with new experimental data on reactions between H2 and well cement and effects on fluid flow and mechanical properties of well cement. 2023.
[18] Hussain A, Al-Hadrami H, Emadi H, Altawati F, Thiyagarajan SR, Watson M. Experimental investigation of wellbore integrity of depleted oil and gas reservoirs for underground hydrogen storage. In: Offshore technology conference; 2022. https://doi.org/10.4043/32003-MS. Houston, Texas, USA.
[19] Shi Z, Jessen K, Tsotsis TT. Impacts of the subsurface storage of natural gas and hydrogen mixtures. Int J Hydrogen Energy 2020;45(15):8757–73. https://doi.org/10.1016/j.ijhydene.2020.01.044.
[20] Boersheim EC, Reitenbach V, Albrecht D, Pudlo D, Ganzer L. Experimental investigation of integrity issues of UGS containing hydrogen. In: SPE europec featured at 81st EAGE conference and exhibition; 2019. https://doi.org/10.2118/195555-MS. London, England, UK.
[21] Shahriar MF, Khanal A, Khan MI, Pandey R. Current status of underground hydrogen storage: perspective from storage loss, infrastructure, economic aspects, and hydrogen economy targets. J Energy Storage 2024;97. https://doi.org/10.1016/j.est.2024.112773. Art no. 112773.
[22] Böttcher N, Görke UJ, Kolditz O, Nagel T. Thermo-mechanical investigation of salt caverns for short-term hydrogen storage. Environ Earth Sci 2017;76(3). https://doi.org/10.1007/s12665-017-6414-2. Art no. 98.
[23] Cheng C, Busch B, Kontny A, Hilgers C. Underground hydrogen storage in sandstone reservoirs: effects of geochemical reactivity of hydrogen on reservoir performance. Int J Hydrogen Energy 2025;105:492–504. https://doi.org/10.1016/j.ijhydene.2025.01.330.
[24] Scrivener K, Snellings R, Lothenbach B, Press C. A practical guide to microstructural analysis of cementitious materials. CRC Press Taylor & Francis Group; 2016.
[25] Bahafid S, Ghabezloo S, Duc M, Faure P, Sulem J. Effect of the hydration temperature on the microstructure of class G cement: CSH composition and density. Cement Concr Res 2017;95:270–81. https://doi.org/10.1016/j.cemconres.2017.02.008.

[26] Hafshejani TM, et al. Effect of polymer-coated silica particles in a Portland cement matrix via in-situ infrared spectroscopy. J Compos Mater 2021;55(4):475–88. https://doi.org/10.1177/0021998320952152.
[27] Binder JL. Analysis of polybutadienes and butadiene-styrene copolymers by infrared spectroscopy. Anal Chem 1954;26(12):1877–82.
[28] Silas RS, Yates J, Thornton V. Determination of unsaturation distribution in polybutadienes by infrared spectrometry. Anal Chem 1959;31(4):529–32.
[29] Lanka ST, Moses NGA, Suppiah RR, Maulianda BT. Physio-chemical interaction of ethylene-vinyl acetate copolymer on bonding ability in the cementing material used for oil and gas well. Petroleum Research 2022;7(3):341–9. https://doi.org/10.1016/j.ptlrs.2021.10.003.
[30] Ramírez-Hernández A, Aguilar-Flores C, Aparicio-Saguilán A. Fingerprint analysis of FTIR spectra of polymers containing vinyl acetate. Dyna 2019;86(209):198–205. https://doi.org/10.15446/dyna.v86n209.77513.
[31] Silva D, Roman H, Gleize P. Evidences of chemical interaction between EVA and hydrating Portland cement. Cement Concr Res 2002;32(9):1383–90. https://doi.org/10.1016/S0008-8846(02)00805-0.
[32] Giraudo N, et al. Calcium silicate phases explained by high-temperature-resistant phosphate probe molecules. Langmuir 2016;32(51):13577–84. https://doi.org/10.1021/acs.langmuir.6b03218.
[33] Horgnies M, Chen J, Bouillon C. Overview about the use of fourier transform infrared spectroscopy to study cementitious materials. WIT Trans Eng Sci 2013;77:251–62. https://doi.org/10.2495/MC130221.
[34] Hughes TL, Methven CM, Jones TG, Pelham SE, Fletcher P, Hall C. Determining cement composition by fourier transform infrared spectroscopy. Adv Cement Base Mater 1995;2(3):91–104. https://doi.org/10.1016/1065-7355(94)00031-X.
[35] Thissen P, Natzeck C, Giraudo N, Weidler P, Wöll C. Hydration of concrete: the first steps. Chem Eur J 2018;24(34):8603–8. https://doi.org/10.1002/chem.201705974.
[36] Mahmood A, Ibuk A, Vogel M, Neuhaus C, Dehn F, Thissen P. Unraveling carbonation and CO2 capture in calcium–silicate–hydrate. ACS Sustainable Chem Eng 2023;11(35):13002–12. https://doi.org/10.1021/acssuschemeng.3c02469.
[37] TerHeege J, Wollenweber J, Naumann M, Pipilikaki P, Vercauteren F. Well integrity of high temperature wells: effect of mineralogical changes on mechanical properties of well cement. In: 53rd U.S. rock mechanics/geomechanics symposium, New York city, New York; 2019. ARMA.
[38] Lu Z, et al. Influences of styrene-acrylate latexes on cement hydration in oil well cement system at different temperatures. Colloids Surf A Physicochem Eng Asp 2016;507:46–57. https://doi.org/10.1016/j.colsurfa.2016.07.082.
[39] Van Gemert D, et al. Cement concrete and concrete–polymer composites: two merging worlds: a report from 11th ICPIC congress in Berlin, 2004. Cement Concr Compos 2005;27(9–10):926–33. https://doi.org/10.1016/j.cemconcomp.2005.05.004.
[40] Wang M, et al. Research on the mechanism of polymer latex modified cement. Constr Build Mater 2016;111:710–8. https://doi.org/10.1016/j.conbuildmat.2016.02.117.
[41] Gelencsér O, et al. Effect of hydrogen on calcite reactivity in sandstone reservoirs: experimental results compared to geochemical modeling predictions. J Energy Storage 2023;61. https://doi.org/10.1016/j.est.2023.106737. Art no. 106737.
[42] Yang Y, Yuan B, Sun Q, Tang X, Yingquan X. Mechanical properties of EVA-Modified cement for underground gas storage. J Nat Gas Sci Eng 2015;27:1846–51. https://doi.org/10.1016/j.jngse.2015.11.013.